

Chapter 5

Residual Stresses Measurement by the Hole-Drilling Technique and DSPI Using the Integral Method with Displacement Coefficients

Armando Albertazzi Jr, Filipe Zanini, Matias Viotti, and Celso Veiga

Abstract The authors developed a portable optical residual stresses measurement device that combines the incremental hole-drilling method with digital speckle pattern interferometry working in polar coordinates. The device is able to measure radial in-plane displacement components around the drilled hole. A set of normalized radial displacement vectors are computed by the Finite Element Method for each hole depth increment, according to the integral method. The radial displacement field around the drilled hole is optically measured and data processed to extract the zero and second order harmonics and fitted by least squares method to the FEM coefficient vectors to quantify the amount of residual stresses in each material layer. The residual stresses profile is then determined for every 0.05 mm. A controlled experiment using a bent plate is used to experimentally evaluate the measurement performance of the developed approach. The results uncertainty are comparable to the strain gauge measurements.

Keywords Residual stresses • Integral method • DSPI • ESPI • Stress measurement

5.1 Introduction

The amount of residual stresses present into a part is very important information in most engineering applications. When combined with loading stresses, residual stresses can bring the material close, or even beyond, the acceptable limits and may result in part failure. Several residual measurement methods are already established: X-ray or neutron diffraction, relaxation, slitting, contouring are among them [1]. Perhaps the most used for in-site applications is the hole-drilling method [2], which is a particular case of relaxation methods.

The hole drilling method consists of progressively drilling a blind hole in the part with residual stresses. As the hole is drilled, a new free surface is built, which progressively releases the amount of residual stresses present in the part. The stress relaxation produces a local deformation around the drilled hole. The deformation is measured and fitted to a model to evaluate residual stresses. The ASTM E837-13a standardizes a procedure to measure residual stresses using a special strain gauge rosette [2].

The hole-drilling method using strain gauges is a time consuming approach, which can reach over 1 h for each measurement point. The authors have developed an integrated device to measure residual stresses in a very practical and faster way using a special optical interferometer in combination with a high speed drilling unit [3–5]. A brief description of the device is presented in this paper. The authors emphasize here the residual stresses calculation approach using the interferometer data.

5.2 Radial In-Plane DSPI Interferometer

The integrated portable device for residuals stresses measurement is described in details in [3–5]. The device uses a special binary diffractive optical element (DOE) to double illuminate a circular area of about 10 mm in diameter. Figure 5.1 helps to describe the working principle of the DSPI interferometer.

A. Albertazzi Jr (✉) • F. Zanini • M. Viotti • C. Veiga
Mechanical Engineering Department, Federal University of Santa Catarina, Florianópolis, SC, Brazil
e-mail: a.abertazzi@ufsc.br

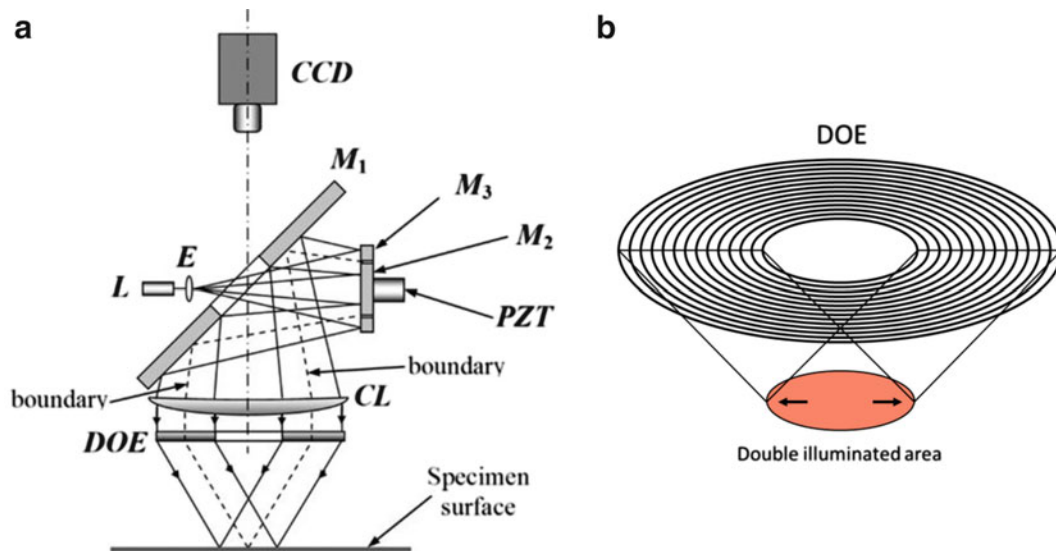


Fig. 5.1 Double illumination speckle interferometer with radial in-plane sensitivity. (a) Optical circuit configurations. (b) Double illumination by an axis-symmetrical diffractive optical element (DOE)

A plane concave lens (E) expands the light coming from a diode laser (L). It passes through the elliptical hole of the mirror M_1 , which forms a 45° angle with the optical axis of the device, illuminating mirrors M_2 and M_3 and being reflected back to the mirror M_1 . Mirror M_1 directs the expanding light to the collimating lens (CL) in order to obtain an annular collimated beam. Finally, the light is diffracted by the DOE mainly in the first diffraction order towards the specimen surface. Residual non-diffracted light or light from other diffraction orders would not be considered troublesome since they are not directed to the central measuring area on the specimen surface. Mirrors M_2 and M_3 are two special circular mirrors. The former is joined to a piezoelectric actuator (PZT) and the later has a circular hole with a diameter slightly larger than diameter of M_2 . Furthermore, mirror M_3 is fixed while M_2 is mobile. The PZT actuator moves the mirror M_2 along its axial direction generating a relative phase difference between the beam reflected by M_2 (central beam) and the one reflected by M_3 (external annular beam). The boundary between both beams is indicated in Fig. 5.1a with dashed lines. According to this figure, it is possible to see that every point over the illuminated area receives only one ray coming from M_2 and only other one from M_3 . Thus, PZT enables the introduction of a relative phase shift to calculate the optical phase distribution by means of phase shifting algorithms. Thus, the central hole placed at M_1 has several functions: (a) to allow that the light coming from the laser source reaches mirrors M_2 and M_3 , (b) to prevent that the laser light reaches directly the specimen surface having triple illumination and (c) to provide a viewing window for the camera (CCD).

Part (b) of Fig. 5.1 shows only one of the diffraction order reaching the double illuminated circular area. The special DOE is a binary circular diffraction grid with a pitch of $1.32 \mu\text{m}$, what result in a diffraction angle of about 30° at a $\lambda = 660 \text{ nm}$ wavelength laser. Since each point on the illuminated area is double illuminated in this special scheme, the sensitivity direction is radial. Therefore, only the displacement component pointing to the circular area center is measured. It is possible to demonstrate and verify that this configuration results in an achromatic interferometer [3].

The authors integrated the radial in-plane DSPI interferometer with a high-speed drilling unit in a portable residual stresses measurement device. Figure 5.2a shows an actual view of the portable device [3–5]. The device has a mechanical base that is firmly attached to the specimen surface by rare earth magnets and three legs with sharp conical tips to avoid relative motions. A motorized mechanical stage is used to automatically exchange the measuring unit and the drilling unit. A measurement software automatically control the test and acquire and process all necessary images to compute the combined stresses profile as a function of the surface depth. Figure 5.2b shows a typical phase difference image after drilling a blind hole in a part with compressive residual stresses with the principal compressive axis near horizontal.

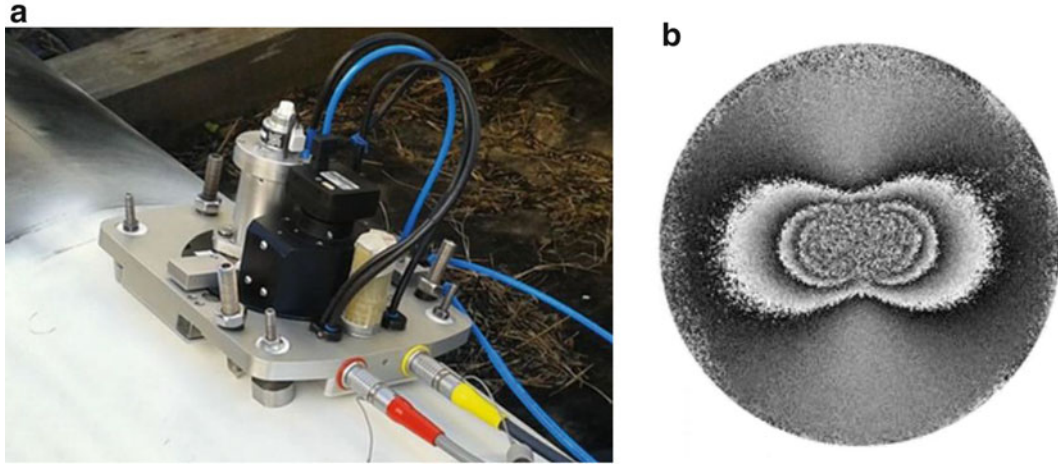


Fig. 5.2 (a) Portable radial in-plane DSPI interferometer combined with a high speed drilling unit to measure combined stresses. (b) A typical radial displacement field due to blind hole drilling measurement

5.3 Residual Stress Calculation

The relationship between the principal residual stresses σ_1, σ_2 , the principal angle β and the radial displacement field $u_r(r, \theta)$ expressed in polar coordinates (r and θ) is in the form of (5.1):

$$u_r(r, \theta) = A(r)(\sigma_1 + \sigma_2) + B(r)(\sigma_1 - \sigma_2) \cos(2\theta - 2\beta) \quad (5.1)$$

$A(r)$ and $B(r)$ are functions of: the radius r , the drilled hole radius r_0 , the hole depth h , and material properties E and ν . There is a closed form for $A(r)$ and $B(r)$ only for a thin infinity plate with uniform stresses and a through hole. For all other cases, only numerical solutions are available. Note that the residual stress sum component does not depend on the polar angle θ . Therefore, it is axially symmetrical. On the other hand, the residual stress difference component depends on the cosine of 2θ and the principal stress direction β .

To quantify the amount for residual stresses in an experiment, two vectors $A(r_k)$ and $B(r_k)$ are extracted from a phase difference map for N discrete radius values (r_k) ranging from $k = 1$ to N and compared with numerically determined reference values. After phase unwrapping, the extraction of $A(r_k)$ and $B(r_k)$ is done through Fourier analysis. The mean radial displacement value for a given radius r_k all way around 2π rad corresponds to the zero order harmonic and to $A(r_k)$. The second harmonic components in cosine $C_2(r_k)$ and the second harmonic components in sine $S_2(r_k)$ are used to compute $B(r_k)$ by $B(r_k) = \sqrt{[(C_2(r_k))^2 + (S_2(r_k))^2]}$ and $\beta_k = \text{Atan}(S_2(r_k)/C_2(r_k))/2$.

Let $a(r_k)$ and $b(r_k)$ be the radial displacement reference values for $A(r_k)$ and $B(r_k)$ respectively. They can be determined through numerical simulations by the finite element method by loading the hole cylindrical surface with an unitary stress and by setting a zero stress at the distant boundary of the object. The finite element used in this analysis belongs to a family of elements of axi-symmetric solids. For the $a(r_k)$ coefficients a uniform biaxial stress field with $\sigma_1 = \sigma_2 = 1.0$ MPa was simulated. For the $b(r_k)$ coefficients calculation the simulation used $\sigma_1 = 1.0$ MPa and $\sigma_2 = -1.0$ MPa. The radius r , ranged from $r_1 = 1.025$ to $r_N = 7.475$ mm with radial increments of 0.025 mm.

The numerical solution of the problem was evaluated by using the ANSYS software. For this reason, two dimensional eight-node elements (PLANE 83) were used. The obtained mesh, shown in Fig. 5.3, had a total of 14,722 elements and 44,601 nodes. Simulations were performed in the same way as an incremental hole-drilling test is executed by following loading recommendations presented in [2]. Hole increments were simulated by drastically reducing the modulus of elasticity at the layers removed by the hole. Twenty steps of 0.05 mm of depth were simulated reaching a final hole depth of 1.00 mm. Displacement coefficients $a_{ij}(r_k)$ and $b_{ij}(r_k)$ were exported as vectors for a future calculations, where i denotes the hole depth increment and j the stress layer count [2, 6]. As an example, Fig. 5.4 shows a plot of these coefficients for the 15th hole step.

To quantify the amount of residual stresses from the measured quantities $A(r_k)$ and $B(r_k)$ a linear behavior was assumed. Therefore, the stress values are proportional to the amount of radial displacements. As an example, let's suppose that $A(r_k)$ is P times bigger than $a(r_k)$. In this case, the sum of residual stresses will be P times bigger than $1.0 + 1.0$ MPa. Since random errors are expected in the experimental values $A(r_k)$, as well as an unexpected bias C may exists, the relationship between

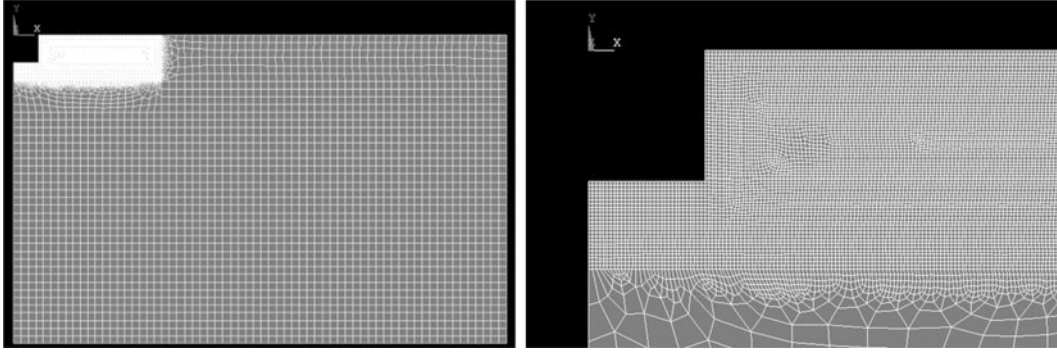
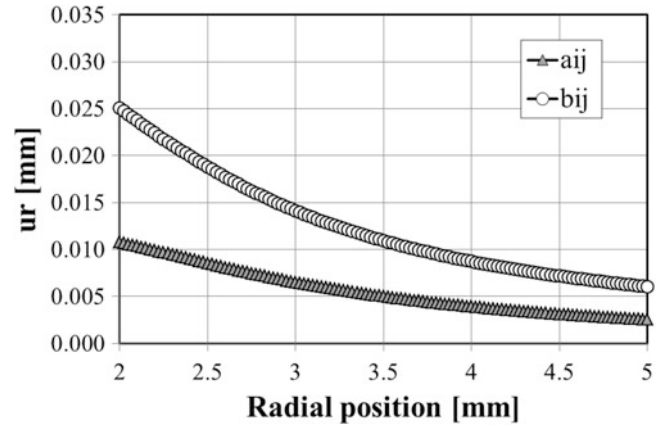


Fig. 5.3 Mesh used during simulation. *Right* part shows a detailed view of the hole region (a) Complete mesh view and (b) Enlarged view of the drilled hole region

Fig. 5.4 Example of $a_{ij}(r_k)$ and $b_{ij}(r_k)$ coefficients



$A(r_k)$ and $a(r_k)$ is in the form of (5.2), where $e(r_k)$ is a random error component. The ij sub indexes were omitted here for simplicity. A similar model is used to relate $B(r_k)$ and $b(r_k)$, but due to space limitation, it will not be described here.

$$A(r_k) = P \cdot a(r_k) + C + e(r_k) \quad (5.2)$$

A least square approach is used to determine P and C . To do that, define the square error function SE by (5.3):

$$SE = \sum_{all r_k} [P \cdot a(r) + C - A(r)]^2 \quad (5.3)$$

The minimum of SE can be found by differentiation of (5.3) to P and C and solving the resulting system of equation. The values for P and C are given by (5.4):

$$C = \frac{\sum_{all r_k} A(r) \cdot \sum_{all r_k} [a(r)]^2 - \sum_{all r_k} [A(r) \cdot a(r)] \cdot \sum_{all r_k} a(r)}{N \sum_{all r_k} [a(r)]^2 - \left[\sum_{all r_k} a(r) \right]^2} \quad \text{and} \quad P = \frac{N \sum_{all r_k} [A(r) \cdot a(r)] - \sum_{all r_k} A(r) \cdot \sum_{all r_k} a(r)}{N \sum_{all r_k} [a(r)]^2 - \left[\sum_{all r_k} a(r) \right]^2} \quad (5.4)$$

To apply the integral method for residual stresses measurement by the incremental hole-drilling technique, the accumulated experimental data for each drilling increment have to be simultaneously fitted to a series of numerical signals. Each signal is related to the hole depth (i) and the stress layer (j). Let $a_{ij}(r)$ denotes the numerical signal computed for the i -depth and j -stress layer [6]. For the first hole depth, the relationship between the experimental data and numerical signal is given by (5.5). The k sub index was omitted for simplicity.

$$A_1(r) = P_1 \cdot a_{11}(r) + C_1 + e_1(r) \quad (5.5)$$

For the second incremental hole depth, the integral method expects to relate the experimental signal to the numerical ones according to (5.6). Since (5.5) alone can determine the value of P_1 , (5.6) involves two unknowns: P_2 the stress value for depth 2 and the additive constant C_2 .

$$A_2(r) = P_1 \cdot a_{21}(r) + P_2 \cdot a_{22}(r) + C_2 + e_2(r) \quad (5.6)$$

For the third hole increment, (5.6) becomes:

$$A_3(r) = P_1 \cdot a_{31}(r) + P_2 \cdot a_{32}(r) + P_3 \cdot a_{33}(r) + C_3 + e_3(r) \quad (5.7)$$

The same idea can be extended for any number of S hole-drilling increments. A general least square solution for the simultaneous system of equations can be developed starting from the sum of the square error given by:

$$\begin{aligned} SE = & \sum_{all\ r} [P_1 \cdot a_{11}(r) + C_1 - A_1(r)]^2 + \sum_{all\ r} [P_1 \cdot a_{21}(r) + P_2 \cdot a_{22}(r) + C_2 - A_2(r)]^2 + \\ & \sum_{all\ r} [P_1 \cdot a_{31}(r) + P_2 \cdot a_{32}(r) + P_3 \cdot a_{33}(r) + C_3 - A_3(r)]^2 + \dots + \sum_{all\ r} [P_1 \cdot a_{S1}(r) + \dots + P_S \cdot a_{SS}(r) + C_S - A_S(r)]^2 \end{aligned} \quad (5.8)$$

The least squares solution for the simultaneous $2S \times 2S$ system can be formed by differentiation of (5.8) to P_1 to P_S and C_1 to C_S and setting all to zero. The $2S$ equations can be easily rearranged to solve the values of the additive constants C_1 to C_S . Since their values have no practical interest, they can be substituted in the equation system that becomes a $S \times S$ system with the S unknowns P_1 to P_S . The resulting matrix system can be written as (5.9) where the elements of the matrix $[X]$ and vectors $\{P\}$ and $\{Y\}$ are given in (5.10).

$$[X]\{P\} = \{Y\} \quad (5.9)$$

Where:

$$\begin{aligned} \{P\} &= \begin{Bmatrix} P_1 \\ \vdots \\ P_S \end{Bmatrix} \\ X_{m,n} &= \sum_{i=Q}^S \left[\sum_{all\ r} (a_{im} \cdot a_{in}) - \frac{1}{N} \sum_{all\ r} a_{im} \cdot \sum_{all\ r} a_{in} \right] \\ Y_m &= \sum_{i=Q}^S \left[\sum_{all\ r} (a_{im} \cdot A_i) - \frac{1}{N} \sum_{all\ r} a_{im} \cdot \sum_{all\ r} A_i \right] \end{aligned} \quad (5.10)$$

The quantity Q is defined as the minimum integer between m or n : $Q = \min(m, n)$.

Usually (5.9) becomes ill-conditioned when S increases. The system (9) can be solved by Tikhonov regularization by (5.11), where α is the regularization factor and $[D]$ is a tri-diagonal second derivative $S \times S$ matrix. The first and last rows of $[D]$ contain zeros; all other rows have $[-1 \ 2 \ -1]$ centered along the diagonal [2, 6].

$$\left([X] - \alpha [D]^T [D] \right) \{P\} = \{Y\} \quad (5.11)$$

Solution of (5.11) result in the principal residual stresses sum for each S drilling increment. The same approach can be applied for $b_{ij}(r_k)$ and $B_{ij}(r_k)$ to determine the principal residual stresses differences as functions of the depth. A combination of both equations allows the determination of both principal residual stresses values individually and for each drilling

increment. More details about the derivation of those equations, as well as, a set of difference equations are the focus of a detailed paper that will be submitted to *Experimental Mechanics* late 2015.

5.4 Experimental Verification

A stress free specimen was bent along a well-defined curved surface as a way to generate reference values for stresses along the specimen depth. All material treatment and geometry were carefully prepared according to recommendations of reference [7]. Figure 5.5 shows a view of the specimen. It is made by: (a) a thick aluminum base with its upper surface machined with a radius of 508 mm, and (b) a thin sheet of aluminum with a thickness of 1.6 mm. The latter part was prepared from a thicker sheet. The final thickness was achieved by machining the material of the surface. Thus, residual stresses generated by the rolling manufacturing process of the original plate were ideally removed resulting in a free-stressed material. The thin sheet was glued to the curved surface introducing a well-defined bending stress profile into the material.

A 1.6 mm diameter drill was used for incremental hole-drilling. A total of $S = 20$ drilling steps of 0.050 mm each were used. For each one a set of four phase shifted images were acquired and used to compute phase values. As a result, 20 phase differences images were obtained always involving the phase differences between the reference state (without the hole) and the actual hole depth. After phase unwrapping, the vectors $A_i(r_k)$ and $B_i(r_k)$ were extracted from each phase difference map of $i = 1$ to 20 and the residual stresses computed using (5.11) for the stresses sum and later for stresses differences. Additional residual stresses measurement were carried out by strain gauge rosettes using the conventional hole-drilling method also with 20 depth increments of 0.050 mm each. Figure 5.6 shows plots of measured residual stresses along the material thickness. S1_DSPI and S2_DSPI are standing for the optically measured principal stresses σ_1 and σ_2 respectively. S1_SG and S2_SG are the plots obtained by strain gauge rosette measurements for σ_1 and σ_2 respectively. All stress profiles were computed after using appropriate Tikhonov regularization coefficients. Figure 5.6 shows a good agreement between measurements obtained by both techniques. The total measurement time for the optical device was about 20 min. For strain gauge measurement the surface was prepared, the strain gauge cemented, wired and the measurement was done by. The total time for strain gauge measurement was about 60 min.

Fig. 5.5 View of the specimen bent over a curved surface and four holes drilled on it

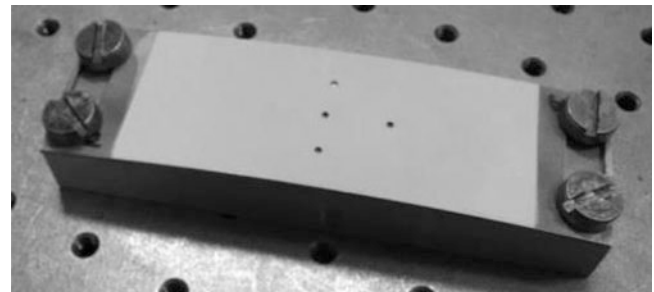
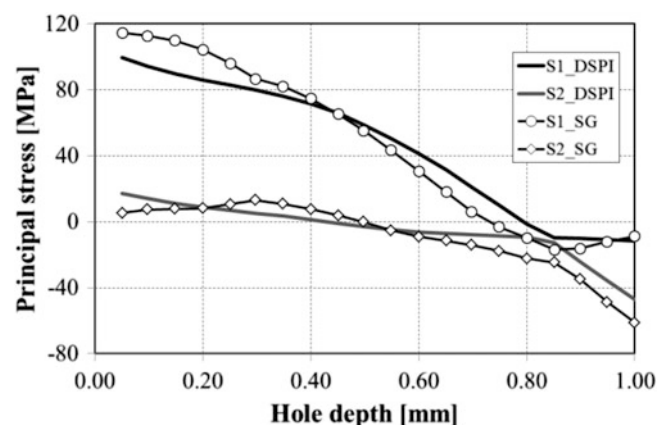


Fig. 5.6 Principal stresses profile results as functions of the hole depth for optical measurement (S1_DSPI and S2_DSPI) and for strain gauge measurement (S1_SG and S2_SG)



5.5 Conclusions

This paper presented a residual stresses calculation model using the incremental method and finite element coefficients expressed in terms of radial displacement along the radius. The measured radial displacement signal is split in two components: the zero and the second order harmonics. The residuals stresses sum is computed from the zero order harmonic using a least squares fitting algorithm with Tikhonov regularizations. The second harmonics are used to compute the residual stresses differences using the same approach, as well as, the principal directions. A bending controlled specimen was used for model validation. The principal stresses profile along the material depth were also measured using strain gauges rosettes. Both signals present a very good agreement and encourage further development of this approach. The total measurement time for the optical device was about 30 % of the time needed for strain gauge measurement.

The use of difference equations as well, as predefined residual stresses profiles, are currently under development and will be present in a paper that has been prepared to be submitted to *Experimental Mechanics* late 2015.

Acknowledgments The authors would like to thanks the financial support of PETROBRAS, CNPq, ANP/PRH 34 and CAPES. They also thanks the encouragement and help of Prof. Gary Schajer on the finite element modeling and the Labmetro team for support.

References

1. G.S. Schajer (ed.), *Practical Residual Stress Measurement Methods*, vol. 7 (Wiley, New York, 2013). ISBN 9781118342374
2. ASTM E837-13, in *Standard Test Method for Determining Residual Stresses by the Hole-Drilling Strain-Gage Method*. Annual Book of ASTM Standards (American Society for Testing and Materials, Philadelphia, 2013)
3. M.R. Viotti, W. Kapp, A. Albertazzi Jr., Achromatic digital speckle pattern interferometer with constant radial in-plane sensitivity by using a diffractive optical element. *Appl. Opt.* **48**(12), 2275–2281 (2009)
4. M.R. Viotti, A. Albertazzi Jr., W.A. Kapp, Experimental comparison between a portable DSPI device with diffractive optical element and a hole drilling strain gage combined system. *Opt. Lasers Eng.* **46**(11), 835–841 (2008)
5. M.R. Viotti, A. Albertazzi Jr., Compact sensor combining digital speckle pattern interferometry and the hole-drilling technique to measure non-uniform residual stress fields. *Opt. Eng.* **52**(10), 101905.1–101905.8 (2013)
6. G.S. Schajer, Measurement of non-uniform residual stresses using the hole-drilling method. Part I - stress calculation procedures. *J. Eng. Mater. Technol.* **110**(4), 338–343 (1988). doi:[10.1115/1.3226059](https://doi.org/10.1115/1.3226059)
7. G.S. Schajer, Hole-drilling residual stress profiling with automated smoothing. *J. Eng. Mater. Technol.* **129**, 440–445 (2007)